Reaction Thermochemistry for Carbon Dioxide Absorption by Aprotic *N*-Heterocyclic Anion Ionic Liquids

Austin N. Keller[†#], Pranav J. Thacker[†#], Michael Baldea[†], Mark A. Stadtherr[†], and Joan F. Brennecke*[†]

[†]McKetta Department of Chemical Engineering, The University of Texas at Austin, Austin, TX 78712 (USA). E-mail: jfb@che.utexas.edu

# These authors contributed equally to this work and are co-first authors.

Keywords

Carbon Capture, Chemisorption, Green Chemistry, Ionic Liquids, Nitrogen Heterocycles

Abstract

Ionic Liquids (ILs) containing aprotic *N*-heterocyclic anions (AHAs) are attractive CO_2 capture solvents. However, CO_2 uptake has only been measured in a limited subset of AHAs (27 tetraalkylphosphonium AHA ILs with 14 unique AHAs). To evaluate the broader range of possible AHA ILs with tetraalkylphosphonium cations, we develop a CO_2 uptake model which is a function of temperature, pressure, and anion-CO_2 reaction enthalpy as calculated using electronic structure methods (DFT). The resulting model accurately describes CO_2 uptake within ± 0.046 moles CO_2 per mole of AHA IL on average. We use this model to predict the CO_2 uptake for ILs of an additional 267 AHAs, whose uptakes have not been measured, for post-combustion carbon capture. Several identified candidates demonstrated similar or greater CO_2 cyclic capacity than the best performing aqueous amines. Additionally, we showed that the anion-CO_2 reaction enthalpy, and hence the anion's basicity, can be correlated with a novel COSMO-RS descriptor—the σ-potential slope of the uncomplexed anion. This requires only a single DFT calculation, roughly halving the computational requirement to construct the uptake model. Lastly, our findings highlight the potential applicability of the σ-potential slope as an electronic descriptor in screening chemical reactivity across various molecular motifs.

I. Introduction

The development of technologies that separate carbon dioxide (CO_2) from air, seawater, flue gas from fossil-fuel combustion, and other industrial process streams is necessary to curtail and, optimistically, to reverse the effects of climate change. Methods developed for CO_2 separation range from adsorption and membrane separation to cryogenic distillation; however, absorption with liquid solvents is currently the most technologically mature.[1] Absorption solvents may either physically dissolve CO_2 or reversibly react with CO_2 to form a new species. Since CO_2 partial pressure is often low, such as in air and in flue gas from natural gas combustion, chemically reactive solvents are preferred. Aqueous amines are the most commonly used chemical solvents;[2] however, they can exhibit poor regeneration thermodynamics due to their strong binding enthalpy with CO_2 and the evaporation of water during solvent regeneration.[3]

Ionic liquids (ILs) have been proposed as alternatives to aqueous amines to overcome these issues. ILs are pure salts in the liquid phase,[4] with melting points below 100 °C.[5] As a result of the strong coulombic interactions inherent in a salt, ILs exhibit negligible volatility, high thermal stability, and low flammability. Additionally, ILs have high tunability, as a result of the many possible anion/cation combinations.[5] ILs can have significant physical solubility for CO_2[6] and can be functionalized with Lewis bases—such as tethered amines,[7] amino acids,[8,9] cation/anion pairs that form carbenes,[10–12] and cation/anion pairs that form ylides[13–15]—to achieve chemical sorption. However, when hydrogen-bond donors are present, the viscosity of these ILs can increase drastically upon complexation with CO_2, due to the hydrogen-bond accepting nature of the oxygens on the complexed CO_2.[16] A special case of amine-derived ILs, those with aprotic *N*-heterocyclic anions (AHAs), capture CO_2 reversibly at a basic nitrogen on the anion to form a carbamate complex, but experience negligible increases in viscosity upon anion complexation with CO_2, due to a lack of hydrogen-bond donors.[17,18]

Designing the optimal IL for a given CO_2 absorption process requires an understanding of the relationship between solvent properties and the economic performance of the process. Fortunately, a handful of process analyses exist to assist with this task. For example, Hospital-Benito et al.[19] studied the performance of six ILs for post-combustion, biogas, and pre-combustion CO_2 capture scenarios and determined that ILs with low solvent and energy requirements had low viscosity and high CO_2 solubility. In later work, Hospital-Benito et al.[20] investigated the direct air

capture (DAC) of CO_2 with ILs, evaluating the sensitivity of energy consumption and economic performance to changes in process conditions and IL reactivity. Moya et al.[21] optimized a process for biogas upgrading with the AHA IL triethyloctylphosphonium 2-cyanopyrrolide ($[P_{2228}][2CNPyr]$) and found that increasing the absorption pressure significantly reduced energy consumption. Hong et al.[22] constructed an equilibrium-based process model using AHA ILs for CO_2 capture from post-combustion flue gas and identified an optimal CO_2 absorption enthalpy target range between −58 and −52 kJ/mol for flue gas from natural gas combined-cycle (NGCC) power plants. Extending this work, Seo et al.[23] developed a non-equilibrium, rate-based model for CO_2 capture from NGCC flue gas with AHA ILs, identifying an optimal absorption enthalpy target of −54.1 kJ/mol and evaluating the effects of viscosity, heat capacity, and molar volume of the AHA IL. These studies suggest that CO_2 absorption with chemically absorbing ILs can become cost-competitive with conventional amine-based technologies when the process design and/or IL absorbent is optimized, and highlight the need for a solvent to have high CO_2 uptake capacity (thus enabling high absorption-desorption cyclic capacity), moderate absorption enthalpy (thereby avoiding excess energy requirements to reverse the uptake reaction and regenerate the IL), as well as low viscosity, molar volume, and heat capacity. However, the analysis cases that include AHA ILs either (1) only consider a single or small set of existing AHA ILs, (2) do not model all five key solvent properties, or (3) perform sensitivity analysis on solvent properties without providing structural insights.

In previous work,[24] we leveraged the available thermophysical property literature data to develop machine-learning models to predict the density, viscosity, and heat capacity of AHA ILs with tetraalkylphosphonium ($[P_{nnnm}]^+$) cations. To meaningfully design ILs based on the property targets presented in the aforementioned process analysis studies, we must be able to model their CO_2 uptake capacity, as a function of temperature and pressure, as well as the closely related property of absorption enthalpy, based solely on chemical structure. Machine-learning modeling of the CO_2 uptake of AHA ILs is particularly difficult because the number of reliable uptake isotherms (those for AHA ILs which are chemically stable and whose data are consistent with the Langmuir-type isotherm model discussed below) available is severely limited (54 isotherms for only 14 different anions).

For the absorption uptake reaction AHA^- (l) + CO_2 (g) ⇌ $AHA–CO_2^-$ (l), density functional theory (DFT) in either the gas-phase or an implicit solvent phase can be used to calculate estimates of relevant species properties (e.g., enthalpy, Gibbs free energy), from which estimates of key reaction properties (e.g., enthalpy of reaction, $\Delta_r H_i^{calc}$; Gibbs free energy of reaction, $\Delta_r G_i^{calc}$, and thus the uptake equilibrium constant) can be determined for an AHA species *i*. If an implicit solvent phase is used, then ideally that phase would have the same electronic properties as the medium of interest (AHA or AHA-CO_2), but these properties are unknown a priori so some arbitrary or default solvent properties must be chosen. Gurkan et al.[25] point out that DFT calculations of CO_2-binding thermochemistry in AHA ILs are relatively insensitive to implicit solvent choice for moderately polar solvents, but Yamada[26] show a significant difference for moderately polar solvents versus water. For this and other reasons discussed below, though estimates of reaction properties using DFT capture experimentally observed trends, their quantitative accuracy can be poor and require correction or calibration. For example, Tang and Wu[27] used gas-phase DFT to estimate $\Delta_r H_i^{calc}$ and found that a correction (adding a constant to the calculated value) was needed to match experimental results. Firaha et al.[28] found that conducting DFT calculations for the AHA and AHA-CO_2 complex in an implicit solvent phase provided moderately good agreement with experimental uptake data after making a correction for the presence of the IL cation trihexyl(tetradecyl)phosphonium ($[P_{66614}]^+$) using COSMO-RS.[29–31] Moya et al.[32] (whose model is used in later works by Palomar and coworkers[20,33]) based the uptake reaction on liquid phase CO_2 and used DFT with all species in an implicit solvent phase. This requires estimation of the Henry's Law constant for the physical solubility of CO_2 in the liquid phase, which was done using COSMO-RS. Since COSMO-RS systematically underestimated the CO_2 solubility a correction factor was introduced to better fit experimental data. They found good agreement with the experimental uptake isotherms of Seo et al.[34] for six of the nine $[P_{66614}][AHA]$ ILs considered. It should be noted, however, that uptake reaction properties (e.g., reaction enthalpy, equilibrium constant) obtained from this approach (treating the CO_2 reactant as liquid phase) will not be directly comparable to most experimental data, which are based on gas phase CO_2. However, since the Moya et al.[32] approach provides uptake predictions for both physical and chemical absorption, it may be advantageous for situations involving significant physical absorption. As explained further below, we are neglecting uptake due to physical absorption in this work.

The efforts described above have only addressed a very limited number of AHA ILs, namely those with the $[P_{66614}]^+$ cation (and only 60 different anions), out of the many possible combinations of anions, cations and their functional moieties, and with only partial success in estimating CO_2 uptake isotherms. With this as motivation, we 1) propose a simple, universal model for predicting CO_2 uptake as a function of temperature and pressure for all $[P_{nnnm}]$[AHA] ILs, requiring only the uptake reaction enthalpy as input; 2) use this model to predict CO_2 uptake, as well as cyclic capacity for a temperature-swing CO_2 capture process, for 267 "in silico" AHAs whose uptakes have never been reliably measured; 3) show how the required input for the model, the uptake reaction enthalpy, can be estimated using a COSMO-RS descriptor, thereby significantly reducing the computational demands of using the new uptake model.

II. Results and Discussion

First, in **Section II.A**, we describe the development and validation of a new, universal Langmuir-type model for the uptake of CO_2 in $[P_{nnnm}]$[AHA] ILs as a function of temperature (T), pressure (P), and $\Delta_r H_i^{\mathrm{calc}}$ as calculated using DFT methods. $[P_{nnnm}]$[AHA] ILs are of primary interest because they have greater thermal stability than AHAs paired with other cations.[35] The model is parameterized using uptake data for the 14 AHAs (in 27 different $[P_{nnnm}]$[AHA] ILs) for which there are reliable experimental data available. Second, in **Section II.B**, we use DFT methods to calculate $\Delta_r H_i^{\mathrm{calc}}$ for 267 additional AHAs and use the results in the new uptake model to determine which of these AHAs are most promising as CO_2 absorbents in a temperature-swing absorption process. Finally, in **Section II.C**, we show how a COSMO-RS descriptor, the slope of the σ-potential in the hydrogen bond acceptor region, can be used to estimate the uptake reaction enthalpy. When combined with the new uptake model, this provides a remarkably simple method for estimating the CO_2 uptake for $[P_{nnnm}]$[AHA] ILs, requiring only a single electronic structure calculation (DFT) for each anion of interest, and eliminating the need for the DFT calculation on the anion-CO_2 complex. COSMO-RS-based descriptors are of particular interest due to the success of recent IL property prediction models[24,36,37] based on them, and the potential to solve multiscale, combined material and process optimization problems using quantitative structure-property relationships (QSPRs) with inputs of uniform material variable descriptors from a single source.

II.A. Development and Validation of a Universal Model for CO_2 Uptake of Tetraalkylphosphonium AHA ILs

The most reliable CO_2 uptake measurements[14,34,38–44] for AHA ILs represent 27 different tetraalkylphosphonium ILs, consisting of 14 different anions and 6 different cations. These are for dry (< 1000 ppm water) AHA ILs. There are 369 data points at pressures up to approximately 1 bar CO_2 and temperatures between 283.15 and 373.15 K (**Table SD2** of the **Supporting Data**). The anions contain both electron-withdrawing and electron-donating groups that influence how strongly the AHA will bind to CO_2. The enthalpy of the AHA species *i* reaction with CO_2 ($\Delta_r H_i^{calc}$) was calculated for these 14 mono- and di-substituted AHAs using DFT methods similar to the implicit solvated approach used by Moya et al.,[32] except with CO_2 in the gas phase. Ground state geometries of AHAs and AHA-CO_2 complexes were first optimized in Gaussian 16[45] using the B3LYP/def2TZVP theory with GD3 empirical dispersion, and an implicit conductor-like polarizable continuum model (CPCM) with water as the solvent. CO_2 was also optimized using a similar DFT protocol, except in the gas phase. The naming conventions for the AHA ILs, along with the detailed DFT protocol for calculating $\Delta_r H_i^{calc}$, are provided in **Section I.A** and **I.B**, respectively, of the **Supporting Information**. The $\Delta_r H_i^{calc}$ values are available in **Table SD1** of the **Supporting Data**. Due to the aromaticity of AHA ILs, all anionic cyclic nitrogen atoms share the negative charge via resonance. Therefore, for an AHA with *n* nitrogen atoms, there are up to *n* possible regioisomers for each AHA-CO_2 complex, depending on symmetry. For this reason, we only consider the lowest energy regioisomer.

Previously, we have found that a Langmuir-type isotherm model (**Equation S1** in the **Supporting Information**) works well[22,25] to describe the CO_2 uptake by chemical absorption of individual AHA ILs, allowing the estimation, for a particular AHA IL *i*, of the standard enthalpy and entropy of the CO_2 uptake reaction ($\Delta_r H_i^{\ominus}$ and $\Delta_r S_i^{\ominus}$, respectively), as well as a maximum uptake capacity factor, C_i (usually between 0.9 and 1.0 moles CO_2 per mole IL), by fit to individual or multiple isotherms for the AHA IL of interest.[34,40,44] The Langmuir-type model describes a situation in which there are specific and independent reaction sites (one per AHA molecule) for chemical absorption, namely a basic nitrogen atom on the anion. CO_2 uptake by physical absorption into the IL will be neglected as it typically accounts for less than 2% of the total uptake at CO_2 pressures up to 1 bar,[34,39] and most carbon capture applications of interest involve CO_2

pressures that are much lower (e.g., flue gas from an NGCC power plant at about 0.04 bar CO_2). Here we explore whether a *single* universal Langmuir-type model can be used to accurately represent, as a function of temperature, pressure, and $\Delta_r H_i^{calc}$, *all* the uptake isotherm data for *all* the 27 [P_{nnnm}][AHA] ILs with reliable uptake data. Since, as discussed above, values from DFT calculations generally capture the correct trends, but can have poor accuracy, we perform a "correction" by assuming a linear relationship between the actual ($\Delta_r H_i^{\ominus}$) and the DFT-calculated ($\Delta_r H_i^{calc}$) values, a generalization of the approach of Tang and Wu.[27] Then, using a procedure described in **Section I.C** of the **Supporting Information**, we develop the universal uptake model for predicting CO_2 uptake by fitting $\Delta_r H_i{}^{calc}$—considering only the most stable regioisomer—to the experimental CO_2 uptake isotherm measurements [14,34,38–44] (**Table SD2** of the **Supporting Data**). After using the van't Hoff equation to capture the dependence of the uptake reaction equilibrium constant on temperature, the Langmuir-type model takes on the form of a logistic function:

$$Z_i = \frac{C}{1 + \exp\left(-\left[\ln(P) - \frac{\Delta_r H_i^{\ominus}}{RT} + \frac{\Delta_r S^{\ominus}}{R}\right]\right)}; \quad \Delta_r H_i^{\ominus} = k\Delta_r H_i^{calc} + c_1 \tag{1}$$

where Z_i is the CO_2 uptake for IL species *i* (moles CO_2 per mole IL), $\Delta_r H_i^{\ominus}$ is the standard enthalpy of reaction for IL *i* with CO_2 (J mol^{-1}), $\Delta_r H_i^{calc}$ is the DFT-calculated enthalpy of reaction estimate for IL *i* with CO_2 (J mol^{-1}), P is the pressure (bar), R is the universal gas constant (8.314 J mol^{-1} K^{-1}), and T is the temperature (K). There are four adjustable parameters: a universal maximum uptake capacity C (moles of CO_2 per mole of IL), a universal standard entropy of reaction $\Delta_r S^{\ominus}$ (J mol^{-1} K^{-1}), the dimensionless parameter k, and the parameter c_1 (J mol^{-1}). The fit of this uptake model to the experimental uptake data is shown in **Figure 1a**, where ILs with different $[P_{nnnm}]^+$ cations are indicated by different colors. With the optimal values of the fitting parameters, this model predicts the uptake data with an average absolute deviation (AAD) of 0.046 mol CO_2/mol IL, which is not significantly greater than the experimental uncertainty (0.02 to 0.04 mol CO_2/mol IL). The optimal values of the four fitted universal parameters are shown in **Table 1**.

Table 1. Optimal values of the four fitted universal parameters for **Eq. (1)**.

Quantity	Value	Units
$\Delta_r S^{\ominus}$	−131	J mol^{-1} K^{-1}
C	0.91	mol CO_2/mol IL
c_1	−11.9	kJ mol^{-1}
k	0.704	—

The optimized value of $\Delta_r S^{\ominus}$ is comparable to that for [P_{66614}][2CNPyr], as measured by Gurkan et al.,[25] and the value for C is in the same range as the values reported for [P_{66614}][AHAs] by Seo et al.[34] With this model we are able to represent the CO_2 uptake capacity as a function of temperature and pressure for all [P_{nnnm}][AHA] ILs, using four temperature-, pressure-, anion-, and cation-independent parameters. Since the data used to determine the parameters in the model include temperatures between 283 K and 373 K, and pressures from 0.013 bar to 2 bar, extrapolating the model to higher or lower temperatures and pressures could result in lower prediction accuracy. For higher pressures, the contribution of physical absorption to the uptake may need to be considered.

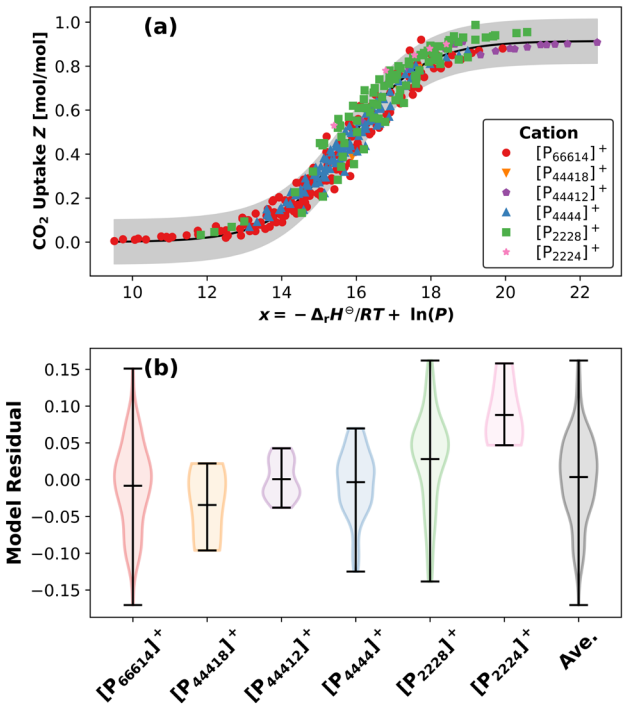

Figure 1: (a) Plot of CO_2 uptakes, Z_i [mol CO_2/mol IL i], for ILs containing six different $[P_{nnnm}]^+$ cations versus $x_i = -\Delta_r H_i^{\ominus}/RT + \ln P$. The black curve is the universal Langmuir-type model (**Eq. 1**) and the gray band is ± 0.1 mol CO_2/mol IL within the model. (b) Violin plots of residual errors for each of the six cations. The gray violin plot is average for the full dataset.

The distribution of residual errors, grouped by cation, is shown in **Figure 1b**. The average residuals for each cation group suggest a weak size effect of the cation. Specifically, the group average residual error follows $[P_{2224}]^+ > [P_{2228}]^+ >$ the average for all cations $\approx [P_{44412}]^+ \approx [P_{4444}]^+ \approx [P_{66614}]^+ > [P_{44418}]^+$. Overall, the model very slightly overpredicts the CO_2 uptake for $[P_{66614}]^+$ AHA ILs and underpredicts CO_2 uptake for $[P_{2228}]^+$ AHA ILs. Higher CO_2 uptake for phosphonium cations with shorter chains was observed by Seo et al.[39] for $[P_{nnnm}]$[2CNPyr] ILs. One hypothesis for this trend [14,42] suggests that the formation of phosphonium ylides is more prominent in $[P_{222n}]^+$ cations than $[P_{66614}]^+$ due to easier accessibility of the α-protons on the alkyl chains. However, recent work by Chaban and Andreeva[46] hypothesized that observed differences in the extent of ylide formation are a function of the rheology of the IL and not the steric accessibility of the α-proton.

II.B. Enthalpy of Reaction and Cyclic Capacity Predictions for In-Silico AHA ILs

In the previous section, we used experimental data for 14 AHAs to develop a universal model for CO_2 uptake as a function of temperature, pressure, and $\Delta_r H_i^{\text{calc}}$ for $[P_{nnnm}]$[AHA] ILs (**Eq. 1**). In this section, we use the same DFT protocol (**Section I.B.** of the **Supporting Information**) to determine $\Delta_r H_i^{\text{calc}}$ values for 267 additional AHAs. After correction to obtain $\Delta_r H_i^{\ominus}$, a detailed analysis of these results is performed. We then consider the CO_2 uptake behavior of the additional AHAs, as predicted from **Eq. 1**, by determining their cyclic capacity for specific absorption and desorption conditions in a temperature-swing absorption process. The additional anions were chosen based on a systematic approach aimed at encompassing a diverse array of azolide structures and their corresponding substituents. The selection process prioritized the inclusion of eight azolide base groups, namely pyrrolide ($[Pyr]^-$), pyrazolide ($[Pyra]^-$), imidazolide ($[Im]^-$), triazolides ($[3Triz]^-$ and $[4Triz]^-$), indolide ($[Indo]^-$), indazolide ($[Inda]^-$), and benzimidazolide ($[BnIm]^-$). Furthermore, mono- and di-substituted anions derived from these base groups, featuring a range of substituents including fluoro (–F), chloro (–Cl), bromo (–Br), iodo (–I), cyano (–CN), methyl ($–CH_3$), trifluoromethyl ($–CF_3$), formyl (–COH), methoxy ($–OCH_3$),

methylthio (–SCH_3), and nitro (–NO_2), were selected. This comprehensive selection strategy ensures a thorough exploration of the reactivity landscape, allowing for insights into the intricate interplay between structural motifs and their chemical behavior. These 267 selected AHAs can be considered as "in silico" from the standpoint of CO_2 uptake since they have no reliable experimental uptake isotherms available. As mentioned previously, the naming conventions for the AHA ILs investigated in this study are provided in **Section I.A** of the **Supporting Information**. Raw (uncorrected) $\Delta_r H_i^{\mathrm{calc}}$ values for forming the additional 267 AHA-CO_2 complexes are available in **Table SD1** of the **Supporting Data**. The corrected reaction enthalpy values ($\Delta_r H_i^{\ominus} = k\,\Delta_r H_i^{calc} + c_1$, using k and c_1 values from the previous section) for all 281 AHAs (including the 14 from the previous section) are given in **Table SD3** in the **Supporting Data**.

The $\Delta_r H_i^{\ominus}$ values for all eight unsubstituted base groups are given in **Table 2**. The magnitudes of these values, which indicate basicity, follow $[Pyr]^-$ >> $[Indo]^-$ > $[Pyra]^-$ > $[Im]^-$ > $[Inda]^-$ > $[BnIm]^-$ > $[4Triz]^-$ > $[3Triz]^-$, a similar order to that reported by Tang and Wu,[27] who performed gas-phase DFT calculations. The key differences are variations in the deactivation strength of the fused six-membered ring and reversal in the order of $[Pyra]^-$ / $[Im]^-$ and $[Inda]^-$ / $[BnIm]^-$. However, experimental results[14] validate our result that the $[Inda]^-$ anion is slightly more basic than $[BnIm]^-$ when paired with a $[P_{66614}]^+$ cation, as evidenced by their CO_2 absorption at both 313 K and 333 K, as well as their experimentally reported enthalpies of reaction (−54 kJ/mol for $[P_{66614}][Inda]$ and −52 kJ/mol for $[P_{66614}][BnIm]$). In all cases, the fusion of a six-membered ring to the corresponding monocyclic base group (e.g., $[Pyr]^-$ → $[Indo]^-$) results in a decrease in $\Delta_r H_i^{\ominus}$ due to further delocalization of the electrons into the larger π-system. However, this effect is much weaker in our implicit-solvent calculations than in the gas-phase calculations of Tang and Wu.[27]

Table 2. Corrected CO_2 reaction enthalpies ($\Delta_r H_i^{\ominus}$) for the most stable regioisomers, for each base group AHA *i*.

Abbreviation (Name)	**Structure**	**CO_2 Reaction Enthalpy ($\Delta_r H_i^{\ominus}$) [kJ/mol]**
$[Pyr]^-$ (Pyrrolide)	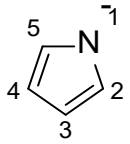	−79.6

[Indo]⁻ (Indolide)	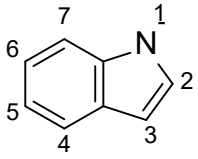	−70.7
[Pyra]⁻ (Pyrazolide)	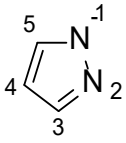	−63.2
[Im]⁻ (Imidazolide)	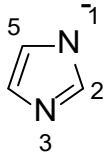	−60.4
[Inda]⁻ (Indazolide)	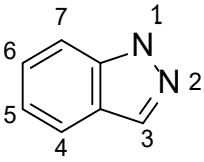	−59.5
[BnIm]⁻ (Benzimidazolide)	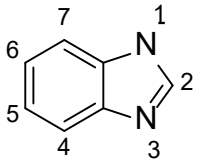	−53.1
[4Triz]⁻ (1,2,4-Triazolide)	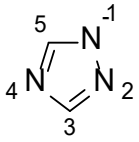	−43.7
[3Triz]⁻ (1,2,3-Triazolide)	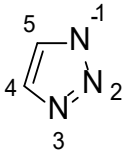	−37.2

The effect of a given functional group on the basicity of an AHA depends both on the electron-withdrawing/donating nature of the substituent and the distance from the reacting nitrogen.[44] We compare the relative effects of all 11 functional groups for each base group by considering the effect of substituting at the 3 position for all anions except for [3Triz]⁻, [Im]⁻, and [BnIm]⁻, which are substituted in the 4 position because the 3 position is unavailable. The deviation from the unsubstituted base group reaction enthalpy is shown in **Figure 2**. From most deactivating to most activating, the series was $-NO_2$ > $-CN$ > $-COH$ > $-CF_3$ > $-I \approx -Br \approx -Cl$ > $-F$ > $-SCH_3$ > $-OCH_3$ > $-CH_3$, and this series was observed for all anion base groups with only a few exceptions. Specifically, it is not clear why $-OCH_3$ is electron withdrawing for imidazolide

and indazolide, but electron donating for pyrazolide, and why the -SCH_3 group has a greater electron withdrawing effect for pyrrolide and indolide than the other AHA base groups. Additionally, the effect of substitution with each functional group in the 3 or 4 position resulted in a similar extent of activation or deactivation of the base group, except for $[BnIm]^-$ which showed significantly less variance because their available 4 position is part of the non-reacting ring.

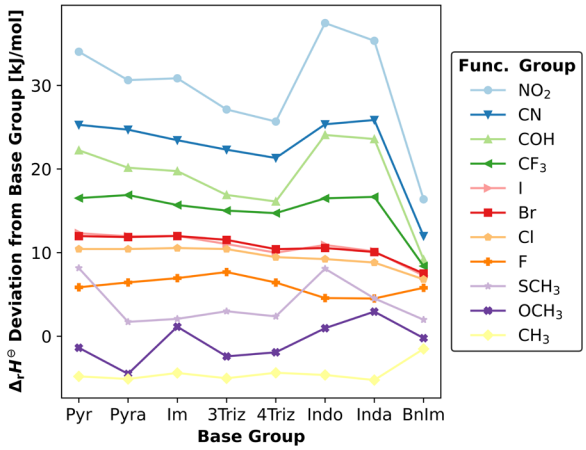

Figure 2. Effect on CO_2 reaction enthalpy ($\Delta_r H_i^\ominus$) of each of 11 functional groups on eight base groups when substituted in the 3 position, or for $[Im]^-$, $[BnIm]^-$, and $[3Triz]^-$ when substituted in the 4 position. Lines are plotted to guide the eye.

The effect of distance from both the reacting nitrogen and its ring can be probed by considering the substitution of each group onto $[Indo]^-$. A plot showing the functionalization position versus $\Delta_r H_i^\ominus$ of the mono-substituted $[Indo]^-$ is shown in **Figure 3**. The impact of substitution on the 5-membered heterocycle with the reactive nitrogen is more noticeable than for the 6-membered homocycle. Specifically, a group's electron withdrawing or donating effect on $\Delta_r H_i^\ominus$ is more prominent when placed at the 3 position compared to the 4, 5, and 6 positions. However, there is consistently a substantial energy penalty associated with functionalization next to the reactive nitrogen atom, specifically at the 2 or 7 positions for indolide-based AHAs. This effect remains significant even for an electron-donating $–CH_3$ group, suggesting that it is independent of the electronic effects induced by the substituent. Therefore, we hypothesize that this energy penalty, when substituents are placed next to the reactive nitrogen, is a result of the introduction of steric strain upon reaction with CO_2. The structure of many of the CO_2 complexes for these cases provided further evidence of this, as these groups caused CO_2 to rotate out of the

plane of the ring to relax van der Waals forces between the bound CO_2 and the functional group. Rotation of the bound CO_2 in this way is known to cause a significant energy penalty due to the loss of resonance[27] between the bound CO_2 (carbamate) and the ring, as indicated by the example given in **Figure 4**.

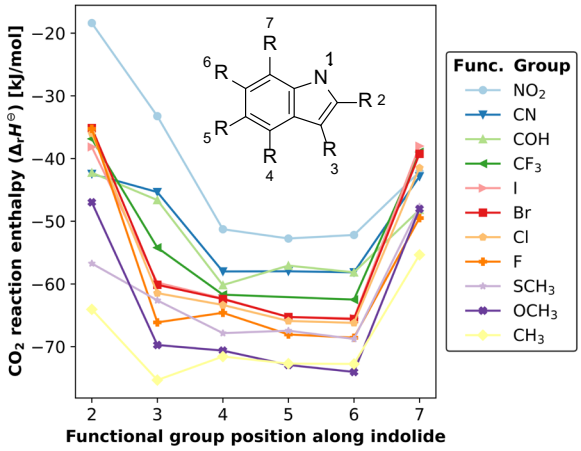

Figure 3. Effect of functional group position on $[Indo]^-$ base group corrected enthalpy of reaction with CO_2 ($\Delta_r H_i^\ominus$). Without any substituents, $[Indo]^-$ has a $\Delta_r H_i^\ominus$ value of −70.7 kJ/mol. Lines are plotted to guide the eye.

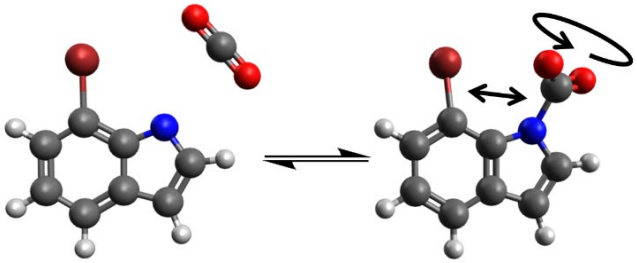

Figure 4. Ball and stick structures showing the rotation of N-C-O bonds out of the plane of the ring due to steric hindrance for the 7-bromoindolide CO_2 complex. Gray color corresponds to carbon, white is hydrogen, blue is nitrogen, red is oxygen, and maroon is bromine.

This steric phenomenon is also observed in the other mono-substituted ions, specifically 2-position functionalized $[Pyr]^-$, $[Im]^-$, and $[BnIm]^-$. Wu et al.[47] attributed steric hindrance as the primary cause of a bending distortion in the C−C≡N bond of a cyano group on $[2CNPyr]^-$, which

we also observed. In general, we expect that the shape and size of each functional group should influence the degree of steric hindrance it produces. The effect of each functional group in a steric position (2-position for $[Pyr]^-$, $[Im]^-$, and $[BnIm]^-$, 2 and 7-positions for $[Indo]^-$) versus the average for that functional group in non-sterically hindering positions is shown in **Figure 5**. Certain functional groups produce greater steric penalties than others. For example, the $-NO_2$ group has a very significant difference between the steric and non-steric positioning due to the bulk and preferred planar alignment of both the carbamate and nitro oxygens. Similarly, the halides ($-F$, $-Cl$, $-Br$, and $-I$), and $-OCH_3$ groups reduce the magnitude of $\Delta_r H_i^{\ominus}$ when in a sterically hindering position. This is hypothesized to be due to greater charge repulsion between the carbamate oxygen and these electronegative functional groups. On the other hand, functional groups that are expected to have distributed charges or low charges, like $-CN$, $-COH$, $-SCH_3$, and $-CH_3$, only modestly reduce the magnitude of $\Delta_r H_i^{\ominus}$.

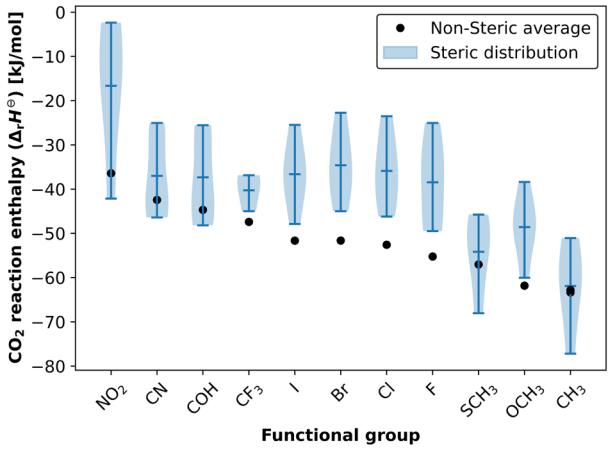

Figure 5. Average predicted $\Delta_r H_i^{\ominus}$ for mono-substituted AHAs with non-sterically hindering functionalization (●) and distribution of $\Delta_r H_i^{\ominus}$ for every base group/steric position combination for each functional group (bands). Marks in the middle of bands are averages and end caps are maximum and minimum values.

The combination of these steric and inductive effects also influences which nitrogen atom is most reactive in the case of anions with multiple cyclic nitrogen atoms. We observed that all $[Inda]^-$ anions preferentially react at the N1 position, except when the 7 position is functionalized, in which case N2 is more favorable. Additionally, there is negligible preference between N1 and N2 for 4-substituted $[Pyra]^-$ anions due to symmetry, but 3-substituted $[Pyra]^-$ anions show regioselectivity for N1.

Using the corrected enthalpies of reaction with CO_2 ($\Delta_r H_i^{\ominus}$) for the 267 new in silico AHA anions, one can predict the CO_2 uptake for each of them at any temperature and pressure using the model (**Eq. 1**) developed in the previous section. With this ability, we can calculate the uptake behavior of AHA ILs in the context of a CO_2 capture process. For this analysis, we consider a process similar to that of Seo et al.[23] consisting of an absorber and stripper (temperature-swing absorption) scheme (see **Figure S2** in the **Supporting Information**) to capture CO_2 from a natural gas-fired power plant. Briefly, in the absorber, flue gas at 1 bar pressure containing 4.08 mol% CO_2 contacts the AHA IL, causing the transfer of CO_2 from the flue gas to the IL. The now CO_2-rich IL is then heated and fed into the stripper (operating at 1 bar pressure) for further heating, with the higher temperature causing the release of CO_2 from the IL. The now regenerated CO_2-lean IL may then be cooled and returned to the absorber. We assume that the IL-CO_2 systems in the absorber and stripper both reach equilibrium, the temperature in each unit is uniform, and the absorber and stripper temperatures are 313.15 K and 443.15 K, respectively. These temperatures are chosen because they are near the optimal absorber and stripper feed conditions reported by Seo et al.[23] However, some ILs may not be stable at this stripper temperature. Using these process conditions, we can calculate the cyclic capacity of the IL, i.e., the difference in CO_2 uptake between the CO_2-rich IL exiting the absorber and the CO_2-lean IL exiting the stripper. Assuming fixed absorber and stripper temperatures, as done here, ILs with larger cyclic capacity will be desired because the molar circulation rate of the IL absorbent decreases with increasing cyclic capacity. However, in a systemwide optimization, with the absorber and stripper temperatures among the decision variables, the IL (or other material used for CO_2 capture) with the largest cyclic capacity will not necessarily be the best, because other IL properties, such as viscosity, density and heat capacity, also influence overall energy consumption and cost.[22,23] Additional details on the hypothetical absorber/stripper scheme and cyclic capacity calculations are available in **Section I. D.** of the **Supporting Information**.

A plot of cyclic capacity versus $\Delta_r H_i^{\ominus}$ for all 281 mono- and di-substituted AHAs is given in **Figure 6**. The bell-curve-like shape is typical of cyclic capacity versus enthalpy-of-capture curves and has a maximum near −54.1 kJ/mol. If CO_2 and the IL bind too weakly, then the CO_2 uptake capacity at absorber conditions (e.g., 313.15 K and 0.0408 bar CO_2 partial pressure) will be too low, i.e., the CO_2 capture target may not be met. If CO_2 and the IL bind too strongly, then

the CO_2 uptake capacity at stripper conditions (e.g., 443.15 K and 1 bar) will be too high, i.e., insufficient CO_2 released in the stripper.

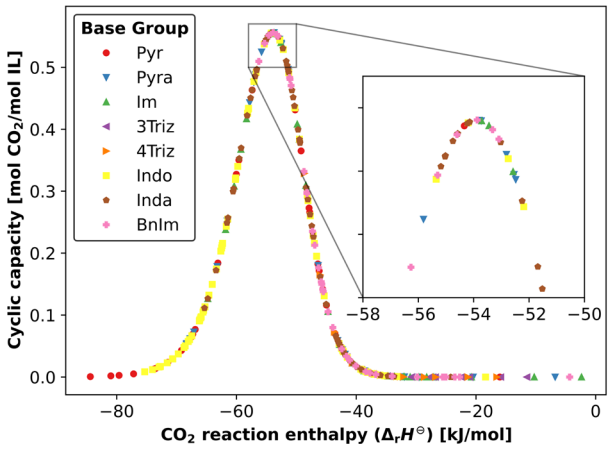

Figure 6. Cyclic capacity under optimal absorber and stripper conditions of Seo et al.[23] versus CO_2 reaction enthalpy ($\Delta_r H_i^{\ominus}$) of 281 AHAs.

A commonly considered AHA for post-combustion carbon capture is $[2CNPyr]^-$,[21–23] and therefore it is chosen as a base case with which to compare others. Promisingly, there are 114 AHA candidates with higher predicted cyclic capacity than the predicted cyclic capacity of the base case AHA, $[2CNPyr]^-$ (0.18 mol/mol, at the specified absorber and stripper conditions). Moreover, there are 18 AHA candidates with cyclic capacities within 2% of the maximum, of which there is published experimental uptake data for only three: $[6BrInda]^-$, $[5BrInda]^-$, and $[BnIm]^-$. The AHA ILs $[P_{2228}][6BrInda]$ and $[P_{2228}][5BrInda]$ were synthesized by Keller et al.[44] and the CO_2 uptake that was measured in that study for $[P_{2228}][6BrInda]$ is predicted by the present model with 5.7% AARD (0.053 mol CO_2/mol IL AAD). ($[P_{2228}][5BrInda]$ was determined to solidify upon uptake of CO_2 and was not considered further, since the Langmuir-type uptake model used here does not account for phase change.) CO_2 uptake measurements have been reported for several $[BnIm]^-$-based ILs[14,38,40,41] and their CO_2 uptakes are predicted by our model with 5.7% AARD (0.040 mol CO_2/mol IL AAD). Additionally, several AHAs within 2% of the maximum cyclic capacity are promising due to low molecular weight, since that may result in a low IL molar volume (as noted above, process optimization studies with AHAs, e.g. Seo et al.,[23] have shown that lower molar volume is economically favorable). By arbitrarily setting a molecular weight cutoff at 110 g/mol, four potential AHA candidates with low molecular weight and high cyclic CO_2 capacity have been

identified, namely 4-fluoroimidazolide ([4FIm]$^-$; 85.06 g/mol), [3CNPyr]$^-$ (91.09 g/mol), 3-chloropyrazolide ([3ClPyra]$^-$; 101.52 g/mol), and 4-chloropyrazolide ([4ClPyra]$^-$; 101.52 g/mol).

For comparison, Bernhardsen and Knuutila[48] report the cyclic capacities of a wide variety of aqueous amine solvents, though based on different process conditions (stripper temperature of 393.15 K, CO_2 feed pressure of 0.15 bar) than considered above. As is common in the aqueous amine context, the cyclic capacities for the aqueous amines considered by Bernhardsen and Knuutila[48] are given on a mass basis and range up to nearly 90 g CO_2/kg solvent. At the same conditions, our predictions for the cyclic capacities of AHA ILs range up to almost 60 g CO_2/kg IL; this is based on choosing the commonly used triethyl(octyl)phosphonium cation ([P_{2228}]$^+$) for purposes of converting the molar uptakes calculated from **Eq. 1** to a mass basis. However, while the mild stripper temperature (393.15 K) used for this comparison is appropriate for aqueous amines (to reduce amine volatility losses and latent heat losses due to water evaporation), for IL absorbents a higher stripper temperature may be used (ILs are nonvolatile and nonaqueous). If a higher stripper temperature of 443.15 K is set when ILs are used, then the AHA IL cyclic capacities range up to 92 g CO_2/kg IL, which is in the same range as the best performing aqueous amines. Additional details of this comparison are presented in **Section I. D** of the **Supporting Information**.

Palomar and coworkers[20,32,33] have also used DFT calculations to estimate CO_2 uptakes of AHA ILs. A main difference between their approach and that presented here is that we use inputs from DFT in a model (**Eq. 1**) fit directly to experimental uptake data, while their model is almost entirely predictive, with a fit only to physical CO_2 solubility of mostly non-AHA ILs to improve the prediction of the Henry's Law constants they require. A comparison of the CO_2 uptakes predicted from their model to those resulting from the model presented here is shown in **Figure S6** of the **Supporting Information**, and a comparison of standard enthalpies of reaction predicted using our model to those predicted by other authors is given in **Table S2** in the **Supporting Information**. Moreover, while the models they propose were developed for AHA ILs with the [P_{66614}]$^+$ cation, our model is fit to data for AHA ILs based on several [P_{nnnm}]$^+$ cations, included those involving the smaller, and thus promising, [P_{2228}]$^+$ cation. Although the AHA IL candidates that Palomar and coworkers have considered are quite limited and the estimates of CO_2 capacity (and cyclic capacity) are significantly less accurate than those presented here (see **Section I. E.** of

Supporting Information), their full process models for both post-combustion CO_2 capture[33] and direct air capture[20] demonstrate the potential of AHA ILs for CO_2 separation. Additional process modeling for AHA ILs shows sensitivity to optimization parameters,[22] cost performance comparable to aqueous piperazine,[23] the effect of feed composition and capture rate,[49] strategies for reducing thermal degradation of the IL,[50] performance in a variable renewable energy environment,[51] and coupled molecular and process optimization.[52] A further advantage of the approach used here, as will be explained in the next section, is that it is possible to reduce the required input from DFT to a single structure optimization for the free, uncomplexed anion.

II. C. Prediction of Reaction Enthalpy from a COSMO-RS Descriptor

Beyond the estimation of CO_2 uptake and binding enthalpy for AHA ILs using *ab initio* (or first-principles) calculations, an additional goal of our work is to develop a framework with which many AHA IL physical properties, including reaction enthalpy and CO_2 uptake, could be estimated using descriptors from a single source. Motivated by previous work[24,36,53,54] from our group and others on applications of COSMO-RS-based descriptors for prediction of physical properties of ILs, we screened molecular descriptors based on the COSMO-RS σ-profiles, σ-moments, and σ-potentials of the unreacted AHAs for correlation to uptake reaction enthalpy. A brief explanation of each of these descriptors is given in **Section I. F.** of the **Supporting Information**. Most features screened showed either poor correlation or poor generalizability across the AHA base groups. However, the slope of the σ-potentials in the hydrogen bond acceptor region was highly correlated to the CO_2 reaction enthalpy and generalized well across all 281 AHAs screened (see details and discussion of underlying theory in **Section I.F.** of the **Supporting Information**), with an overall R^2 of 0.768 without consideration of steric effects. A plot showing the correlation between $\Delta_r H_i^{\ominus}$, the corrected DFT-calculated CO_2 reaction enthalpy (as used in previous sections) and σ-potential slope for all 281 AHAs is shown in **Figure 7** (solid black line). This means that $\Delta_r H_i^{\ominus}$ and, subsequently, CO_2 capacity as a function of temperature and pressure (using **Eq. 1**), can be predicted from a single DFT calculation for the AHA anion. One does *not* have to do an electronic structure calculation for the AHA-CO_2 complex, thus effectively cutting the computational requirement in half.

In cases where functional groups adjacent to the reacting nitrogen are not −H, that is, in cases where there is a potential intramolecular interaction between a bound CO_2 and the functional

group, the σ-potential slope model gives an overestimate of $\Delta_r H_i^{\ominus}$. We hypothesize that, while the σ-potential slope descriptor adequately represents the inductive effects of functionalization of the AHA, it falls short of capturing steric effects. In fact, constructing separate models for steric (80) and non-steric (201) AHAs gives R^2 values of 0.713 and 0.949, respectively (blue dashed-dot and red dashed lines in **Figure 7**, respectively).

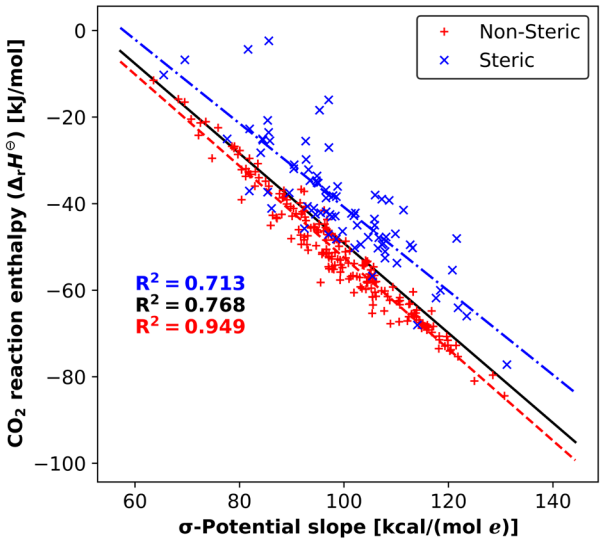

Figure 7. Plot of corrected CO_2 reaction enthalpy ($\Delta_r H_i^{\ominus}$) in kJ/mol versus σ-potential slope for AHA *i* in kcal/(mol *e*) where *e* is the elementary charge, 1.602×10^{-19} coulombs. The solid black line is best fit for all data, the red dashed line is for non-steric cases where the functional group(s) adjacent to the reaction site are −H, and the blue dashed-dot line is for steric cases where the functional group(s) adjacent to the reaction site are not −H.

To account for the steric effect, a correction term was added to the model which adjusts the predicted enthalpy of the reaction of the AHA with CO_2 for the steric species as a function of the O−C−N−C dihedral angle (inset of **Figure 8**). As discussed earlier, this angle is a result of the rotation of CO_2, as needed to relax the steric strain between CO_2 and the functional group; however, this rotation is electronically unfavorable as it breaks the resonance between CO_2 and the rest of the ion. Since there are multiple regimes of the steric effect due to the rotational energy penalty being nonlinear[27] and the varied nature of the substituents studied, a piecewise linear function was used for the residual steric term, and its development, as well as the full steric-corrected model, is described in **Section I. G.** of the **Supporting Information**. The final steric-

corrected model fits the data well with an overall R^2 of 0.937 and AAD of 2.7 kJ/mol. A parity plot of the corrected DFT-calculated CO_2 reaction enthalpy ($\Delta_r H^{\ominus}$) versus the enthalpy from the steric-corrected σ-potential slope model is shown in **Figure 8**.

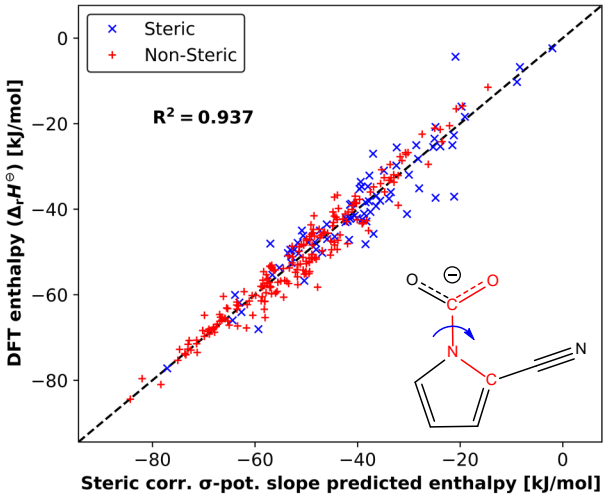

Figure 8. Parity plot of corrected DFT-calculated CO_2 reaction enthalpy ($\Delta_r H_i^{\ominus}$) versus steric-corrected σ-potential slope predicted enthalpy for AHA *i*.

We also explored whether a simpler charge descriptor could perform as effectively as the slope of the σ-potential. Building on the insights of Wang et al.,[55] who correlated CO_2 absorption enthalpy of phenolate-based ILs with Mulliken charges on the reactive oxygen, we attempted to replicate this correlation with AHAs. Therefore, we evaluated the correlation between Mulliken charges on the reactive nitrogen of 281 AHAs and their respective $\Delta_r H_i^{\ominus}$ values. The Mulliken charge of the reactive nitrogen showed a strong correlation within some individual base groups; e.g., $[Pyra]^-$ and $[4Triz]^-$ had R^2 values of 0.928 and 0.909, respectively. However, the correlation was weak for all three bicyclic AHA base groups—$[BnIm]^-$, $[Indo]^-$, and $[Inda]^-$, with R^2 values of 0.209, 0.086, and 0.067, respectively. Furthermore, the performance of a single Mulliken charge model generalized to all base groups was rather poor. Even when considering only non-steric cases, the correlation using Mulliken charge yielded an R^2 value of 0.171, compared to the 0.949 value for the σ-potential slope model. Additional analysis and calculation details involving the Mulliken charge model are available in **Section I. H.** of the **Supporting Information**.

Given the novelty of the σ-potential slope descriptor, we also tested its generalizability. We sought to assess the suitability of the non-steric σ-potential slope model, which is based on

201 non-sterically hindered AHAs (**Eq. S7** of the **Supporting Information**), for estimating $\Delta_r H_i^{\ominus}$ of non-AHA bases. To this extent, we performed DFT calculations on the unreacted and reacted base for phenolate, 4-bromophenolate, 4-trifluoromethylphenolate, and 4-methoxyphenolate ($[PhO]^-$, $[4BrPhO]^-$, $[4CF_3PhO]^-$, and $[4OCH_3PhO]^-$, respectively), hydroxide ($[HO]^-$), methoxide ($[CH_3O]^-$), acetate ($[AcO]^-$), and piperazine (PZ) to calculate their $\Delta_r H_i^{\ominus}$ values, and determined the slope of their σ-potential curves from the electronic structure calculation for the unreacted base. The $\Delta_r H_i^{\ominus}$ values are for the direct addition of CO_2 to the bases. Therefore, it is only an analog of basicity, because the mechanisms by which many of these bases react with CO_2 involve multiple steps and/or water. Additional details on these calculations are provided in **Section I. I.** of the **Supporting Information**. The results, illustrated in **Figure 9** and tabulated in **Table S4**, demonstrate a strong correlation between $\Delta_r H_i^{\ominus}$ and σ-potential slopes for these non-AHA bases, closely matching the previously developed relationship for the 201 non-steric AHAs. This compelling correlation underscores the applicability and broad utility of the σ-potential slope as a versatile descriptor in this domain. It should be noted that the $[AcO]^-$ anion is an outlier, and the correlation (represented by the red dashed line) was developed excluding this anion. With the information currently available, the reason for $[AcO]^-$ being an outlier remains unclear.

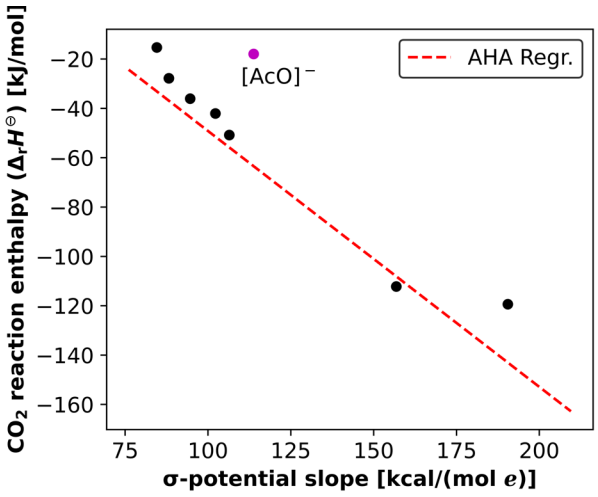

Figure 9. CO_2 addition enthalpy versus σ-potential slope of 8 non-AHA bases (●) plotted against the correlation of **Eq. S7** (--). $[AcO]^-$ (●) is an outlier and was excluded from the regression.

Lastly, we sought to validate the utility of the σ-potential slope by comparing it with previous findings in the field. Wang et al.[55] recently established a notable correlation between the

CO_2 absorption capacity of phenolate ILs and the conjugate acid dissociation constant (pK_a) of the anion bases in a non-aqueous solvent, dimethyl sulfoxide (DMSO). Interestingly, we observed a similarly good correlation between the slope of the σ-potential for the bases and the pK_a of the conjugate acid in the IL [DBUH][TfO][56] (R^2 of 0.866), in a polar nonaqueous solvent DMSO[57] (R^2 of 0.936), and in water[57] (R^2 of 0.707) for a set of bases including the aforementioned non-AHA bases (where data was available), as well as the AHAs $[Im]^-$, $[Pyra]^-$, $[4Triz]^-$, and $[3Triz]^-$. The pK_a in each solvent of the conjugate acid of each base versus the σ-potential slope feature of each base is shown in **Figure 10** and tabulated in **Table S4**. Similar to the correlation for the enthalpy of reaction with CO_2, the $[AcO]^-$ anion is an outlier when correlating pK_a and σ-potential slope. Establishing a straightforward correlation between an electronic descriptor derived from commonly tabulated COSMO-RS data and the pK_a of the species could be a valuable analytical tool as it can offer significant insights into chemical reactivity and reaction mechanisms beyond the realm of carbon capture chemistry.

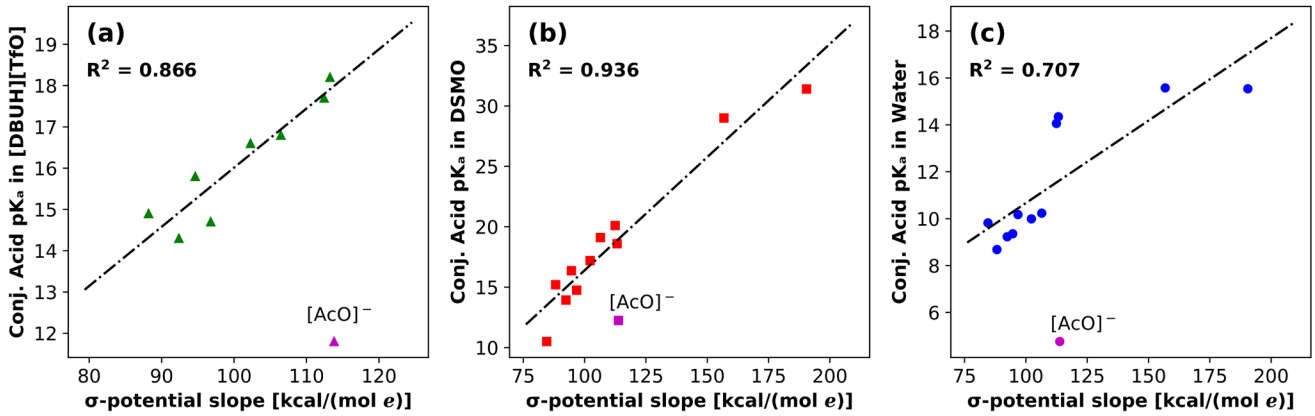

Figure 10. Conjugate acid pK_a in [DBUH][TfO] (a), DMSO (b), and water (c) versus σ-potential slope of AHA and non-AHA bases. $[AcO]^-$ (▲, ●, ■) is an outlier and was excluded from the regressions.

III. Conclusions

We have developed a simple, universal model to predict CO_2 uptake as a function of temperature and pressure for tetraalkylphosphonium-based ILs containing aprotic *N*-heterocyclic anions (AHAs). The only required input is the enthalpy of the reaction between the anion and CO_2, which can be obtained from electronic structure calculations of the anion and anion-CO_2 complex in an implicit solvent phase. Four temperature-, pressure-, anion- and cation-independent parameters were fit to the available experimental data for 27 $[P_{nnnm}][AHA]$ ILs (14 unique anions). The model

results in a modest AAD of 0.046 mol CO_2/mol IL, which is in the range of typical experimental uncertainties. With this model, CO_2 capacities were predicted for a total of 281 different AHA anions, allowing us to identify several anions with significant potential for post-combustion carbon capture in NGCC power systems. In particular, we identified four monocyclic anions (4-fluoroimidazolide [4FIm]$^-$, 3-cyanopyrrolide [3CNPyr]$^-$, 3-chloropyrazolide ([3ClPyra]$^-$, and 4-chloropyrazolide ([4ClPyra]$^-$) with low molecular weights, and with cyclic capacity very near the optimal value for the capture of CO_2 from NGCC power plant flue gas, representing a roughly 3-fold increase in cyclic capacity over the base case AHA IL, [P_{2228}][2CNPyr]. Furthermore, we have shown that the enthalpy of reaction between the anion and CO_2 is correlated with the σ-potential slope, a COSMO-RS-based descriptor that requires a DFT calculation for only the anion, and not the anion-CO_2 complex, thus reducing the computational work compared to earlier methods by roughly a factor of two. Using a piecewise linear correction for sterically hindered anions, the correlation between the σ-potential slope and the enthalpy of reaction has an R^2 of 0.937 and AAD of 2.7 kJ/mol, identifying the σ-potential slope as a robust descriptor for the estimation of the CO_2 uptake enthalpy. Moreover, we also found this descriptor to correlate well with conjugate acid pK_a values, for AHAs and certain non-AHA bases. Consequently, we find the σ-potential slope to be a promising tool for swiftly screening the acid/base equilibria important for a variety of chemical processes.

Supporting Information: Description of computational procedures and theory (PDF); uncorrected and corrected standard enthalpy of reaction values, sigma-profiles, sigma-potentials, experimental CO_2 uptake data, fitting variables including sigma-potential slope, steric classifier, and O-C-N-C dihedral, and Mulliken charges (XLXS); optimized structure files (XYZ).

Acknowledgements: This work was supported by the University of Texas Energy Institute under the Fueling a Sustainable Energy Transition (FSET) program. It was also partially funded by the Robert A. Welch Foundation (grant no. F-1945-20180324) as well as by the National Science Foundation (NSF) under the Environmental Convergence Opportunities in Chemical, Bioengineering, Environmental, and Transport Systems program (ECO-CBET). We acknowledge the Texas Advanced Computing Center (TACC) at The University of Texas at Austin for providing HPC and storage resources which have contributed to the research results reported within this paper.

IV. References

(1) Leung, D. Y. C.; Caramanna, G.; Maroto-Valer, M. M. An Overview of Current Status of Carbon Dioxide Capture and Storage Technologies. *Renewable and Sustainable Energy Reviews* **2014**, *39*, 426–443. https://doi.org/10.1016/j.rser.2014.07.093.

(2) Mumford, K. A.; Wu, Y.; Smith, K. H.; Stevens, G. W. Review of Solvent Based Carbon-Dioxide Capture Technologies. *Front. Chem. Sci. Eng.* **2015**, *9* (2), 125–141. https://doi.org/10.1007/s11705-015-1514-6.

(3) Rochelle, G. T. Conventional Amine Scrubbing for CO_2 Capture. In *Absorption-Based Post-combustion Capture of Carbon Dioxide*; Feron, P. H. M., Ed.; Woodhead Publishing, 2016; pp 35–67. https://doi.org/10.1016/B978-0-08-100514-9.00003-2.

(4) Welton, T. Ionic Liquids: A Brief History. *Biophys Rev* **2018**, *10* (3), 691–706. https://doi.org/10.1007/s12551-018-0419-2.

(5) Brennecke, J. F.; Maginn, E. J. Ionic Liquids: Innovative Fluids for Chemical Processing. *AIChE Journal* **2001**, *47* (11), 2384–2389. https://doi.org/10.1002/aic.690471102.

(6) Aghaie, M.; Rezaei, N.; Zendehboudi, S. A Systematic Review on CO_2 Capture with Ionic Liquids: Current Status and Future Prospects. *Renewable and Sustainable Energy Reviews* **2018**, *96*, 502–525. https://doi.org/10.1016/j.rser.2018.07.004.

(7) Bates, E. D.; Mayton, R. D.; Ntai, I.; Davis, J. H. CO_2 Capture by a Task-Specific Ionic Liquid. *J. Am. Chem. Soc.* **2002**, *124* (6), 926–927. https://doi.org/10.1021/ja017593d.

(8) Gurkan, B. E.; de la Fuente, J. C.; Mindrup, E. M.; Ficke, L. E.; Goodrich, B. F.; Price, E. A.; Schneider, W. F.; Brennecke, J. F. Equimolar CO_2 Absorption by Anion-Functionalized Ionic Liquids. *J. Am. Chem. Soc.* **2010**, *132* (7), 2116–2117. https://doi.org/10.1021/ja909305t.

(9) Firaha, D. S.; Kirchner, B. Tuning the Carbon Dioxide Absorption in Amino Acid Ionic Liquids. *ChemSusChem* **2016**, *9* (13), 1591–1599. https://doi.org/10.1002/cssc.201600126.

(10) Shiflett, M. B.; Drew, D. W.; Cantini, R. A.; Yokozeki, A. Carbon Dioxide Capture Using Ionic Liquid 1-Butyl-3-Methylimidazolium Acetate. *Energy Fuels* **2010**, *24* (10), 5781–5789. https://doi.org/10.1021/ef100868a.

(11) Yokozeki, A.; Shiflett, M. B.; Junk, C. P.; Grieco, L. M.; Foo, T. Physical and Chemical Absorptions of Carbon Dioxide in Room-Temperature Ionic Liquids. *J. Phys. Chem. B* **2008**, *112* (51), 16654–16663. https://doi.org/10.1021/jp805784u.

(12) Seo, S.; DeSilva, M. A.; Brennecke, J. F. Physical Properties and CO_2 Reaction Pathway of 1-Ethyl-3-Methylimidazolium Ionic Liquids with Aprotic Heterocyclic Anions. *J. Phys. Chem. B* **2014**, *118* (51), 14870–14879. https://doi.org/10.1021/jp509583c.

(13) Scaglione, N.; Avila, J.; Bakis, E.; Padua, A.; Gomes, M. C. Alkylphosphonium Carboxylate Ionic Liquids with Tuned Microscopic Structures and Properties. *Phys. Chem. Chem. Phys.* **2023**, *25* (22), 15325–15339. https://doi.org/10.1039/D3CP01009K.

(14) Gohndrone, T. R.; Song, T.; DeSilva, M. A.; Brennecke, J. F. Quantification of Ylide Formation in Phosphonium-Based Ionic Liquids Reacted with CO_2. *J. Phys. Chem. B* **2021**, acs.jpcb.1c03546. https://doi.org/10.1021/acs.jpcb.1c03546.

(15) Yeadon, D. J.; Jacquemin, J.; Plechkova, N. V.; Maréchal, M.; Seddon, K. R. Induced Protic Behaviour in Aprotonic Ionic Liquids by Anion Basicity for Efficient Carbon Dioxide Capture. *ChemPhysChem* **2020**, *21* (13), 1369–1374. https://doi.org/10.1002/cphc.202000320.

(16) Gutowski, K. E.; Maginn, E. J. Amine-Functionalized Task-Specific Ionic Liquids: A Mechanistic Explanation for the Dramatic Increase in Viscosity upon Complexation with CO_2 from Molecular Simulation. *J. Am. Chem. Soc.* **2008**, *130* (44), 14690–14704. https://doi.org/10.1021/ja804654b.
(17) Brennecke, J. F.; Gurkan, B. E. Ionic Liquids for CO_2 Capture and Emission Reduction. *J. Phys. Chem. Lett.* **2010**, *1* (24), 3459–3464. https://doi.org/10.1021/jz1014828.
(18) Wang, C.; Luo, X.; Luo, H.; Jiang, D.; Li, H.; Dai, S. Tuning the Basicity of Ionic Liquids for Equimolar CO_2 Capture. *Angewandte Chemie International Edition* **2011**, *50* (21), 4918–4922. https://doi.org/10.1002/anie.201008151.
(19) Hospital-Benito, D.; Lemus, J.; Moya, C.; Santiago, R.; Palomar, J. Process Analysis Overview of Ionic Liquids on CO_2 Chemical Capture. *Chemical Engineering Journal* **2020**, *390*, 124509. https://doi.org/10.1016/j.cej.2020.124509.
(20) Hospital-Benito, D.; Moya, C.; Gazzani, M.; Palomar, J. Direct Air Capture Based on Ionic Liquids: From Molecular Design to Process Assessment. *Chemical Engineering Journal* **2023**, 143630. https://doi.org/10.1016/j.cej.2023.143630.
(21) Moya, C.; Santiago, R.; Hospital-Benito, D.; Lemus, J.; Palomar, J. Design of Biogas Upgrading Processes Based on Ionic Liquids. *Chemical Engineering Journal* **2022**, *428*, 132103. https://doi.org/10.1016/j.cej.2021.132103.
(22) Hong, B.; Simoni, L. D.; Bennett, J. E.; Brennecke, J. F.; Stadtherr, M. A. Simultaneous Process and Material Design for Aprotic *N*-Heterocyclic Anion Ionic Liquids in Postcombustion CO_2 Capture. *Ind. Eng. Chem. Res.* **2016**, *55* (30), 8432–8449. https://doi.org/10.1021/acs.iecr.6b01919.
(23) Seo, K.; Tsay, C.; Hong, B.; Edgar, T. F.; Stadtherr, M. A.; Baldea, M. Rate-Based Process Optimization and Sensitivity Analysis for Ionic-Liquid-Based Post-Combustion Carbon Capture. *ACS Sustainable Chem. Eng.* **2020**, *8* (27), 10242–10258. https://doi.org/10.1021/acssuschemeng.0c03061.
(24) Keller, A. N.; Kelkar, P.; Baldea, M.; Stadtherr, M. A.; Brennecke, J. F. Thermophysical Property Prediction of Anion-Functionalized Ionic Liquids for CO_2 Capture. *Journal of Molecular Liquids* **2024**, *393*, 123634. https://doi.org/10.1016/j.molliq.2023.123634.
(25) Gurkan, B.; Goodrich, B. F.; Mindrup, E. M.; Ficke, L. E.; Massel, M.; Seo, S.; Senftle, T. P.; Wu, H.; Glaser, M. F.; Shah, J. K.; Maginn, E. J.; Brennecke, J. F.; Schneider, W. F. Molecular Design of High Capacity, Low Viscosity, Chemically Tunable Ionic Liquids for CO_2 Capture. *J. Phys. Chem. Lett.* **2010**, *1* (24), 3494–3499. https://doi.org/10.1021/jz101533k.
(26) Yamada, H. Comparison of Solvation Effects on CO_2 Capture with Aqueous Amine Solutions and Amine-Functionalized Ionic Liquids. *J. Phys. Chem. B* **2016**, *120* (40), 10563–10568. https://doi.org/10.1021/acs.jpcb.6b07860.
(27) Tang, H.; Wu, C. Reactivity of Azole Anions with CO_2 from the DFT Perspective. *ChemSusChem* **2013**, *6* (6), 1050–1056. https://doi.org/10.1002/cssc.201200986.
(28) Firaha, D. S.; Hollóczki, O.; Kirchner, B. Computer-Aided Design of Ionic Liquids as CO_2 Absorbents. *Angewandte Chemie International Edition* **2015**, *54* (27), 7805–7809. https://doi.org/10.1002/anie.201502296.
(29) Klamt, A. Conductor-like Screening Model for Real Solvents: A New Approach to the Quantitative Calculation of Solvation Phenomena. *J. Phys. Chem.* **1995**, *99* (7), 2224–2235. https://doi.org/10.1021/j100007a062.

(30) Klamt, A.; Jonas, V.; Bürger, T.; Lohrenz, J. C. W. Refinement and Parametrization of COSMO-RS. *J. Phys. Chem. A* **1998**, *102* (26), 5074–5085. https://doi.org/10.1021/jp980017s.
(31) Klamt, A.; Eckert, F.; Arlt, W. COSMO-RS: An Alternative to Simulation for Calculating Thermodynamic Properties of Liquid Mixtures. *Annu. Rev. Chem. Biomol. Eng.* **2010**, *1* (1), 101–122. https://doi.org/10.1146/annurev-chembioeng-073009-100903.
(32) Moya, C.; Hospital-Benito, D.; Santiago, R.; Lemus, J.; Palomar, J. Prediction of CO_2 Chemical Absorption Isotherms for Ionic Liquid Design by DFT/COSMO-RS Calculations. *Chemical Engineering Journal Advances* **2020**, *4*, 100038. https://doi.org/10.1016/j.ceja.2020.100038.
(33) Hospital-Benito, D.; Lemus, J.; Moya, C.; Santiago, R.; Palomar, J. Improvement of CO_2 Capture Processes by Tailoring the Reaction Enthalpy of Aprotic N-Heterocyclic Anion-Based Ionic Liquids. *Chemical Engineering Journal Advances* **2022**, *10*, 100291. https://doi.org/10.1016/j.ceja.2022.100291.
(34) Seo, S.; Quiroz-Guzman, M.; DeSilva, M. A.; Lee, T. B.; Huang, Y.; Goodrich, B. F.; Schneider, W. F.; Brennecke, J. F. Chemically Tunable Ionic Liquids with Aprotic Heterocyclic Anion (AHA) for CO_2 Capture. *J. Phys. Chem. B* **2014**, *118* (21), 5740–5751. https://doi.org/10.1021/jp502279w.
(35) Fillion, J. J.; Xia, H.; Desilva, M. A.; Quiroz-Guzman, M.; Brennecke, J. F. Phase Transitions, Decomposition Temperatures, Viscosities, and Densities of Phosphonium, Ammonium, and Imidazolium Ionic Liquids with Aprotic Heterocyclic Anions. *J. Chem. Eng. Data* **2016**, *61* (8), 2897–2914. https://doi.org/10.1021/acs.jced.6b00269.
(36) Nordness, O.; Kelkar, P.; Lyu, Y.; Baldea, M.; Stadtherr, M. A.; Brennecke, J. F. Predicting Thermophysical Properties of Dialkylimidazolium Ionic Liquids from Sigma Profiles. *Journal of Molecular Liquids* **2021**, *334*, 116019. https://doi.org/10.1016/j.molliq.2021.116019.
(37) Abranches, D. O.; Zhang, Y.; Maginn, E. J.; Colón, Y. J. Sigma Profiles in Deep Learning: Towards a Universal Molecular Descriptor. *Chem. Commun.* **2022**, *58* (37), 5630–5633. https://doi.org/10.1039/D2CC01549H.
(38) Seo, S.; Simoni, L. D.; Ma, M.; DeSilva, M. A.; Huang, Y.; Stadtherr, M. A.; Brennecke, J. F. Phase-Change Ionic Liquids for Postcombustion CO_2 Capture. *Energy Fuels* **2014**, *28* (9), 5968–5977. https://doi.org/10.1021/ef501374x.
(39) Seo, S.; DeSilva, M. A.; Xia, H.; Brennecke, J. F. Effect of Cation on Physical Properties and CO_2 Solubility for Phosphonium-Based Ionic Liquids with 2-Cyanopyrrolide Anions. *J. Phys. Chem. B* **2015**, *119* (35), 11807–11814. https://doi.org/10.1021/acs.jpcb.5b05733.
(40) Song, T.; Avelar Bonilla, G. M.; Morales-Collazo, O.; Lubben, M. J.; Brennecke, J. F. Recyclability of Encapsulated Ionic Liquids for Post-Combustion CO_2 Capture. *Ind. Eng. Chem. Res.* **2019**, *58* (12), 4997–5007. https://doi.org/10.1021/acs.iecr.9b00251.
(41) Bennett, J. E. Acid Gas and Nitrogen Solubility in Ionic Liquids for Carbon Capture Applications. Doctoral Dissertation, University of Notre Dame, Notre Dame, Indiana, 2014.
(42) Oh, S.; Morales-Collazo, O.; Keller, A. N.; Brennecke, J. F. Cation–Anion and Anion–CO_2 Interactions in Triethyl(Octyl)Phosphonium Ionic Liquids with Aprotic Heterocyclic Anions (AHAs). *J. Phys. Chem. B* **2020**, *124* (40), 8877–8887. https://doi.org/10.1021/acs.jpcb.0c06374.

(43) Fillion, J. J.; Bennett, J. E.; Brennecke, J. F. The Viscosity and Density of Ionic Liquid + Tetraglyme Mixtures and the Effect of Tetraglyme on CO_2 Solubility. *J. Chem. Eng. Data* **2017**, *62* (2), 608–622. https://doi.org/10.1021/acs.jced.6b00596.
(44) Keller, A. N.; Bentley, C. L.; Morales-Collazo, O.; Brennecke, J. F. Design and Characterization of Aprotic *N*-Heterocyclic Anion Ionic Liquids for Carbon Capture. *J. Chem. Eng. Data* **2022**, *67* (2), 375–384. https://doi.org/10.1021/acs.jced.1c00827.
(45) Frisch, M. J.; Trucks, G. W.; Schlegel, H. B.; Scuseria, G. E.; Robb, M. A.; Cheeseman, J. R.; Scalmani, G.; Barone, V.; Petersson, G. A.; Nakatsuji, H.; Li, X.; Caricato, M.; Marenich, A. V.; Bloino, J.; Janesko, B. G.; Gomperts, R.; Mennucci, B.; Hratchian, H. P.; Ortiz, J. V.; Izmaylov, A. F.; Sonnenberg, J. L.; Williams-Young, D.; Ding, F.; Lipparini, F.; Egidi, F.; Goings, J.; Peng, B.; Petrone, A.; Henderson, T.; Ranasinghe, D.; Zakrzewski, V. G.; Gao, J.; Rega, N.; Zheng, G.; Liang, W.; Hada, M.; Ehara, M.; Toyota, K.; Fukuda, R.; Hasegawa, J.; Ishida, M.; Nakajima, T.; Honda, Y.; Kitao, O.; Nakai, H.; Vreven, T.; Throssell, K.; Montgomery, J. A., Jr.; Peralta, J. E.; Ogliaro, F.; Bearpark, M. J.; Heyd, J. J.; Brothers, E. N.; Kudin, K. N.; Staroverov, V. N.; Keith, T. A.; Kobayashi, R.; Normand, J.; Raghavachari, K.; Rendell, A. P.; Burant, J. C.; Iyengar, S. S.; Tomasi, J.; Cossi, M.; Millam, J. M.; Klene, M.; Adamo, C.; Cammi, R.; Ochterski, J. W.; Martin, R. L.; Morokuma, K.; Farkas, O.; Foresman, J. B.; Fox, D. J. Gaussian 16, 2016.
(46) Chaban, V. V.; Andreeva, N. A. From Tetraalkylphosphonium Ionic Liquids to Phosphonium Ylides: How the Ionic Sizes Influence Carbon Dioxide Capture? *Journal of Molecular Liquids* **2023**, *382*, 121948. https://doi.org/10.1016/j.molliq.2023.121948.
(47) Wu, C.; Senftle, T. P.; Schneider, W. F. First-Principles-Guided Design of Ionic Liquids for CO_2 Capture. *Phys. Chem. Chem. Phys.* **2012**, *14* (38), 13163–13170. https://doi.org/10.1039/C2CP41769C.
(48) Bernhardsen, I. M.; Knuutila, H. K. A Review of Potential Amine Solvents for CO_2 Absorption Process: Absorption Capacity, Cyclic Capacity and pKa. *International Journal of Greenhouse Gas Control* **2017**, *61*, 27–48. https://doi.org/10.1016/j.ijggc.2017.03.021.
(49) Seo, K.; Tsay, C.; Edgar, T. F.; Stadtherr, M. A.; Baldea, M. Economic Optimization of Carbon Capture Processes Using Ionic Liquids: Toward Flexibility in Capture Rate and Feed Composition. *ACS Sustainable Chem. Eng.* **2021**, *9* (13), 4823–4839. https://doi.org/10.1021/acssuschemeng.1c00066.
(50) Seo, K.; Chen, Z.; Edgar, T. F.; Brennecke, J. F.; Stadtherr, M. A.; Baldea, M. Modeling and Optimization of Ionic Liquid-Based Carbon Capture Process Using a Thin-Film Unit. *Computers & Chemical Engineering* **2021**, *155*, 107522. https://doi.org/10.1016/j.compchemeng.2021.107522.
(51) Seo, K.; Retnanto, A. P.; Martorell, J. L.; Edgar, T. F.; Stadtherr, M. A.; Baldea, M. Simultaneous Design and Operational Optimization for Flexible Carbon Capture Process Using Ionic Liquids. *Computers & Chemical Engineering* **2023**, 108344. https://doi.org/10.1016/j.compchemeng.2023.108344.
(52) Seo, K.; Brennecke, J. F.; Edgar, T. F.; Stadtherr, M. A.; Baldea, M. Multiscale Design of Ionic Liquid Solvents and CO_2 Capture Processes for High-Pressure Point Sources. *ACS Sustainable Chem. Eng.* **2024**, *12* (2), 706–715. https://doi.org/10.1021/acssuschemeng.3c03697.
(53) Zhao, Y.; Zeng, S.; Huang, Y.; Afzal, R. M.; Zhang, X. Estimation of Heat Capacity of Ionic Liquids Using $S_{\sigma\text{-profile}}$ Molecular Descriptors. *Ind. Eng. Chem. Res.* **2015**, *54* (51), 12987–12992. https://doi.org/10.1021/acs.iecr.5b03576.

(54) Zhao, Y.; Huang, Y.; Zhang, X.; Zhang, S. A Quantitative Prediction of the Viscosity of Ionic Liquids Using $S_{\sigma\text{-profile}}$ Molecular Descriptors. *Phys. Chem. Chem. Phys.* **2015**, *17* (5), 3761–3767. https://doi.org/10.1039/C4CP04712E.
(55) Wang, C.; Luo, H.; Li, H.; Zhu, X.; Yu, B.; Dai, S. Tuning the Physicochemical Properties of Diverse Phenolic Ionic Liquids for Equimolar CO_2 Capture by the Substituent on the Anion. *Chemistry – A European Journal* **2012**, *18* (7), 2153–2160. https://doi.org/10.1002/chem.201103092.
(56) Gao, F.; Wang, Z.; Ji, P.; Cheng, J.-P. CO_2 Absorption by DBU-Based Protic Ionic Liquids: Basicity of Anion Dictates the Absorption Capacity and Mechanism. *Frontiers in Chemistry* **2019**, *6*.
(57) J.-D. Yang, X.-S. Xue, P. Ji, X. Li, J.-P. Cheng, **2018**. "Internet Bond-energy Databank (pKa and BDE)--iBonD". http://ibond.nankai.edu.cn/ . Version 2.0.

For Table of Content Use Only

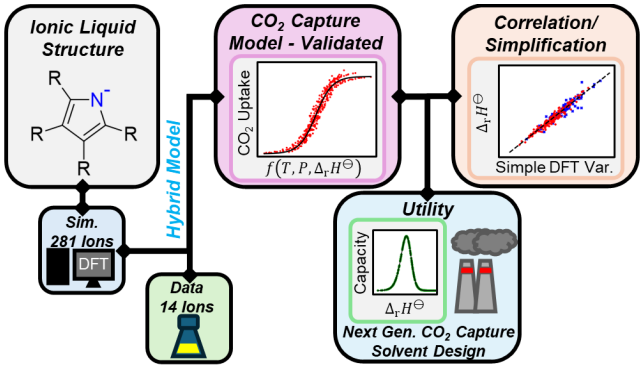

Synopsis

A universal model requiring a single first principles calculation allows design of improved ionic liquids for more sustainable carbon capture processes.